Journal of Sustainable Development of Energy, Water and Environment Systems

http://www.sdewes.org/jsdewes

Year 2026, Volume 14, Issue 3, 1140719

Original Research Article

Numerical analysis of blade design for enhanced wind turbine performance

M. Lazarevikj*[*1], M. Uler-Zefikj, I. Zdravkovska, E. Vasileska Tuteska, V. Iliev, R. V. Filkoski

[1] Faculty of Mechanical Engineering – Skopje, Ss. Cyril and Methodius University in Skopje, Skopje, North Macedonia

e

Cite as: Lazarevikj, M., Uler-Zefikj, M., Zdravkovska, I., Vasileska Tuteska, E., Iliev, V., Filkoski, R. V., Numerical analysis of blade design for enhanced wind turbine performance, J.sustain. dev. energy water environ. syst., 14(3), 1140719, 2026, DOI: https://doi.org/10.13044/j.sdewes.d14.0719

-mail: marija.lazarevikj@mf.edu.mk

ABSTRACT

The transition to renewable energy sources is increasingly urgent as fossil fuels remain a major source of greenhouse gas emissions. Wind energy represents a promising option due to its low cost, environmental benefits, and continuous technological advancements. Although several high-potential locations have been identified in North Macedonia, wind resources remain underutilized and studies on turbine designs adapted to local conditions are limited. This study investigates blade design for a selected site in North Macedonia through a comparative evaluation of several blade geometry analytical approaches for a horizontal-axis wind turbine, together with an iterative refinement aimed at improving geometric feasibility, all based on the Blade Element Momentum theory. Airfoil selection considered both aerodynamic and structural requirements along the blade span, using a thicker DU-97 profile in the inboard region and FFA-W3 airfoils toward the mid and outer blade sections. Numerical simulations were performed to analyse aerodynamic performance, loading characteristics, and expected energy production, providing insight into blade configurations suitable for site-specific wind conditions in North Macedonia.

KEYWORDS

Blade design, Geometric parameters, Numerical analysis, Renewable energy sources, Wind turbine.

INTRODUCTION

The global focus on renewable energy resources has increased significantly in recent years, driven by rising environmental concerns, increasing energy demands and the depletion of fossil fuel resources [1]. The urgency to transition to cleaner energy systems is emphasized by the growing impact of climate change and the need for sustainable development across all sectors [2], [3]. A key strategic framework guiding this transition is the Net Zero Emissions by 2050 Scenario (NZE Scenario), proposed by the International Energy Agency (IEA), which provides a detailed roadmap and norms for the global energy sector to achieve net-zero CO_2 emissions by the year 2050, requiring a transformation in the way energy is produced, distributed and consumed [4]. According to the IEA, the global adoption of renewable fuels and technologies must nearly double by 2030 to remain on track with the NZE pathway, demanding acceleration in the deployment of renewable energy technologies. Different sources of renewable energy include biomass, solar, geothermal, hydropower and wind [5]. The IEA forecasts that solar

* Corresponding author

UNCORRECTED PROOF

photovoltaics and wind power plants will account for approximately 95% of the total renewable capacity additions through the end of this decade, mainly due to their improving cost competitiveness and wide-scale adaptability across almost all countries [4]. Critical analysis of their environmental impact can be found in literature works that may serve as a valuable resource for developers, policymakers and decision-makers when planning future solar and wind farms [6].

Focusing on the renewable energy technologies currently experiencing the most rapid growth, wind energy stands out due to its high conversion efficiency and operational advantages [7], [8]. The theoretical maximum energy conversion efficiency of a wind turbine is defined by the Betz limit, which sets an upper bound of 59.3% for the amount of kinetic energy that can be extracted from the wind flow. In practice, modern wind turbine designs can achieve conversion efficiencies in the range of 40% to 50% under optimal conditions [9]. In contrast, commercial solar photovoltaic panels typically achieve conversion efficiencies between 15% and 22%, depending on the technology and environmental conditions [10]. Furthermore, wind energy is characterized by low operating and maintenance costs, and near-zero greenhouse gas emissions during operation, making it one of the cleanest sources of large-scale energy generation [11]. Unlike fossil fuel sources such as coal that require transportation and treatment before processing, wind energy can be harnessed directly at suitable geographic locations. Wind power has been established as a non-polluting and renewable energy source, with growing attention directed toward its integration into modern energy systems [12]. According to forecast by IEA in 2024, the growth trajectory of wind energy is set to accelerate significantly. Onshore wind cumulative capacity is expected to almost double between 2023 and 2030, reaching approximately 846 GW, driven by policy reforms and technological improvements such as improved aerodynamic rotor designs, high-performance composite blade materials, the integration of advanced energy storage solutions, etc. [4].

Despite this global momentum, RNM remains significantly behind in using its wind energy potential. Currently, wind power contributes with only 2.76% or 82.4 MW of the total installed energy capacity in the country, with this entire output coming from three wind power plants. Recent study showed that the region has several locations with high wind speeds and strong technical potential for wind power generation [13]. This underutilized potential presents a critical gap and requires research and development efforts aimed at using North Macedonia's wind energy resources.

In response to these requirements and advantages, significant research efforts have been directed toward advancing wind power generation technologies. Recent studies have emphasized on increasing the efficiency of wind turbines, with particular focus on improving the aerodynamic and structural performance of their components, especially on the rotor blades since they are a critical element in overall turbine effectiveness [14]. They function as the interface between the air kinetic energy and the turbine mechanical-electrical conversion system and are responsible for capturing the wind and transferring the torque to the rotor hub [15]. Their effectiveness is governed by key geometrical and design parameters [16]. Studies have shown that even minor blade design modifications can lead to substantial improvements in turbine performance, particularly under non-ideal wind conditions [17]. For instance, optimized airfoil geometries and variable pitch designs have been demonstrated to boost the energy efficiency of wind turbines [18]. In parallel, advancements in materials science, such as the use of reinforced composite materials, have contributed to lighter, stronger and more durable blades, reducing fatigue and increasing lifespan without compromising aerodynamic performance [19]. As noted by Schaffarczyk [20], the design of turbine blades is not just a component-level optimization task, but a multidisciplinary challenge that integrates fluid dynamics, structural mechanics and control systems.

However, despite the global progress in this area, there are currently no studies in RNM that address blade design optimization. Existing research in the region has primarily focused on other aspects of wind energy, such as power prediction [21], wind farm layout optimization

UNCORRECTED PROOF

[22], wind resource assessment [23], condition monitoring and fault detection [24], as well as performance and sustainability evaluations [25].

To the authors' knowledge, no prior research study has explored the aerodynamic and structural optimization of wind turbine blades designed and evaluated for specific sites in RNM. The contribution of this study is threefold. First, it provides a systematic comparative analysis of several classical wind turbine blade geometry formulations under identical aerodynamic and geometric assumptions representative of an IEC Class III turbine. Second, an iterative BEM-based refinement is introduced to obtain a more realistic and manufacturable blade geometry while maintaining comparable aerodynamic efficiency. Third, by analysing both aerodynamic performance and thrust loading characteristics, the study identifies the design approach that offers the most balanced compromise between efficiency and structural loading for turbines operating in moderate wind regimes.

There are various types of wind turbines. All wind turbines consist of some basic design elements, such as the rotor, gearbox, generator, transformer, control system, yaw drive, tower and the basement. Wind turbines can be categorized based on various criteria. According to the orientation of their axis, they are classified as horizontal-axis or vertical-axis wind turbines [26]. Based on wind speed, they fall into three categories: low-speed wind turbines (Reynolds number (Re) $< 10^3$), medium-speed wind turbines ($10^3 < Re < 10^5$) and high-speed wind turbines ($Re > 10^5$) [27].

In terms of their position relative to wind flow, wind turbines are either upwind-positioned or downwind-positioned [28]. Based on the rotor size, there are micro-scale wind turbines (0.1 m), small-scale wind turbines (0.1 m-1 m), mid-scale wind turbines (1 m-5 m) and large-scale wind turbines (greater than 5m) [29]. Depending on aerodynamic principles, they can be classified as lift-type or drag-type. The number of blades further differentiates them into single-bladed or multi-bladed wind turbines [30]. Finally, based on installation location, wind turbines are either onshore or offshore [31].

Blade design consists of both aerodynamic and structural components. The aerodynamic component focuses on optimizing performance by first selecting an appropriate standardized airfoil model and then defining the blade aerodynamic shape parameters. The airfoil design focuses on selecting the best profile, while shape parameters determine how the blade is formed along its length to maximize efficiency. The structural component ensures mechanical integrity by choosing suitable blade materials and designing sectional configurations [32]. These steps ensure the blade can withstand aerodynamic and mechanical loads while maintaining efficiency and longevity.

Over the years, various airfoil families have been specifically developed for wind energy applications, each offering distinct advantages based on operating conditions and design objectives. Early wind turbine designs commonly utilize the traditional National Advisory Committee for Aeronautics (NACA) airfoils known as NACA series [33]. To enhance wind turbine blade performance, several specialized airfoil families have been developed. The National Renewable Energy Laboratory (NREL) has made significant contributions to wind turbine airfoil development through the S-series, which are specifically designed for horizontal-axis wind turbines (HAWTs) [34]. The airfoils designed by the Swedish Aeronautical Research Institute (FFA) are known as FFA-W series and offer high-lift characteristics and improved performance in turbulent wind conditions [35], [36]. Similarly, the Delft University of Technology created the airfoils known as DU series that have been optimized for large wind turbines, offering high aerodynamic efficiency and structural robustness [37]. The Risø National Laboratory in Denmark made the Risø series (A1, B1 etc.) which are designed to minimize aerodynamic noise while maintaining high energy conversion efficiency [38], [39]. The NPU-WA series of airfoils are one of the latest produced and they are developed by Northwestern Polytechnical University. They are designed for megawatt-class wind turbines, featuring high lift-to-drag ratios at elevated Reynolds numbers and high design lift coefficients [40]. The University of Illinois at Urbana-Champaign in collaboration

UNCORRECTED PROOF

with NASA designed and tested SG (Selig-Gutmann) airfoil family for low Reynolds number applications [41].

A comparative aerodynamic analysis of conventional NACA airfoils and other types of airfoils highlights some key differences. Studies show that while the NACA 4412 airfoil achieves a higher lift coefficient than the NREL S823, its lift decreases significantly beyond an 8° angle of attack (AoA), whereas the NREL S823 maintains more stable lift characteristics. Additionally, NACA airfoils generally exhibit lower drag coefficients across all AoA, indicating higher aerodynamic efficiency but reduced stability compared to NREL airfoils [33]. A similar trend is observed in vertical-axis wind turbines (VAWTs). Traditional NACA airfoils, such as NACA 0015 and NACA 0021, achieve higher power output at greater tip-speed ratios, while NREL airfoils like S814 and S825 generate more torque at lower tip-speed ratios. This makes NREL airfoils well-suited for self-starting Darrieus turbines, though they experience greater efficiency losses at higher tip-speed ratios [42]. Comparative studies on airfoil geometries, including NACA 0012, NACA 2412 and SG6043, reveal that the AoA significantly affects lift and drag. The maximum lift coefficient occurs at 15°, while the minimum drag coefficient is at 0°. The lift-to-drag ratio peaks at 5° for SG6043 and 10° for NACA 0012 and NACA 2412. Unlike the NACA airfoils, SG6043 exhibits asymmetric velocity and turbulence, creating a stronger wake region [43]. Wind tunnel tests compared the FFA-W3-241, FFA-W3-301 and NACA 63-430 airfoils. The findings indicated that FFA-W3 airfoils are better suited for the inboard sections of wind turbine blades, both with and without vortex generators. In contrast, the NACA 63-430 airfoil exhibited less favourable aerodynamic characteristics under similar conditions [36].

The development of the airfoil series throughout the years is given in Figure 1. The selection of an optimal airfoil depends on various factors, including wind speed conditions, blade size, manufacturing constraints and operational requirements. Traditional NACA airfoils continue to be widely utilized due to the abundance of experimental data, performance charts and design guides available, which can be beneficial when comparing theoretical results with practical wind tunnel tests [44], [45]. The NACA four-digit and five-digit series have straightforward mathematical formulations, are relatively simple to use, and their construction is based on clear parameters such as camber, thickness and chord [46].

ACCEPTED PROOF

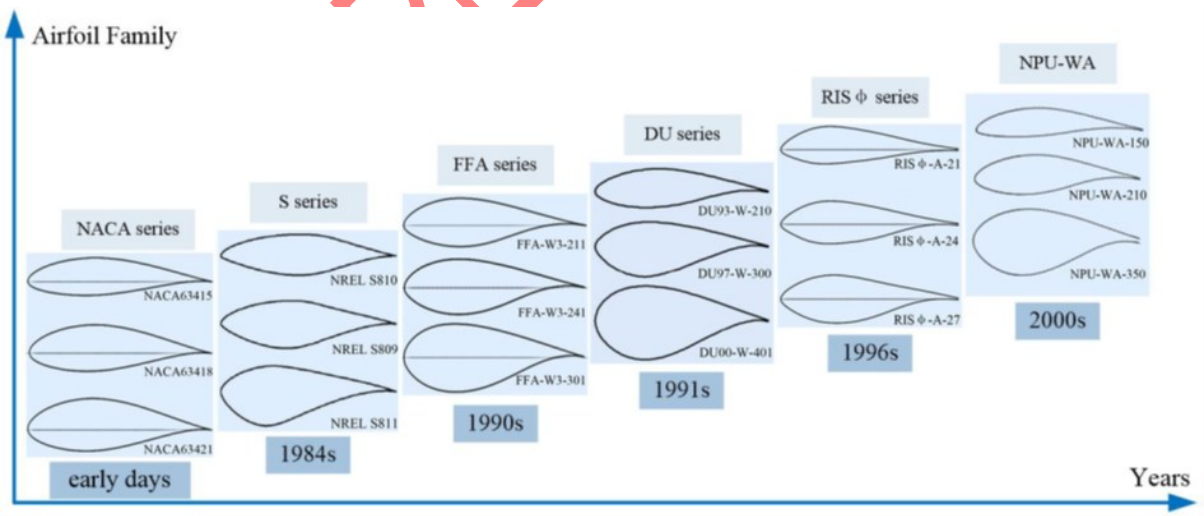

Figure 1. Development of airfoil series throughout the years [2]

The application of computational tools with numerical methods has enabled more precise and efficient blade optimization strategies, allowing designers to evaluate the aerodynamic performance across a wide range of operating conditions. Over the years, several numerical methods have been developed to simulate wind turbine aerodynamics, including vortex methods, 3D viscous-inviscid interaction techniques, Computational Fluid Dynamics (CFD)

and Blade Element Momentum (BEM) [47]. Among these, the BEM method has emerged as the most practical and widely used technique in industrial wind turbine design due to its balance between computational efficiency and accuracy in performance prediction under a variety of operating conditions [48]. Compared to BEM, CFD has higher fidelity since it includes the physics that is neglected by BEM [49], it provides the possibility of 3D modelling and simulations, as well as the display of the entire flow field including the unsteady flow. Also, the distribution of parameters such as pressure, density, temperature, can be taken into consideration using CFD model. The key advantage of BEM over full CFD simulations, that represents the reason for its application in this research, lies in its reduced computational cost and rapid iteration capability, making it highly suitable for early-stage rotor design and parametric studies. It allows for quick exploration of multiple design configurations, which can later be validated through high-fidelity CFD or wind tunnel testing [50]. However, BEM has its limitations arising from the neglection of the interactions between the blade elements and the three-dimensional flow field around the blade, as well as the error accumulation in iterative calculations [51]. Also, the classical BEM calculation cannot predict wind turbine performance at high wind speeds due to flow separation phenomenon [50].

Although more advanced blade optimization approaches have been developed in recent years, including CFD-based methods and models incorporating three-dimensional flow corrections or stall-delay effects, classical BEM design formulations remain widely used for preliminary rotor design due to their transparency and low computational cost. These analytical approaches provide clear relationships between aerodynamic assumptions and resulting blade geometry, which makes them particularly suitable for comparative studies. Considering that this is an early-stage analysis aiming to provide primary information about the blade design that does not require high precision simulations with great cost, the BEM method was selected and used as an appropriate tool for the current research requirements.

Table 1 presents a summary of the most commonly used wind turbine simulation softwares along with their key features.

Table 1. Most commonly used wind turbine simulation software and their key features

Software	Developer/Organization	Main Purpose	Key Features	Open Source
QBlade	TU Berlin	Blade design and aerodynamic simulation using BEM	Airfoil generation, rotor design, BEM analysis, visualization	Yes
OpenFAST	NREL (National Renewable Energy Laboratory)	Full wind turbine aeroelastic simulation	Modular, supports multi-physics, structural, control systems	Yes
Bladed	DNV	Industrial-grade turbine design and certification	Industry-standard, certified calculations, supports floating turbines	No
AeroDyn	NREL (as a module in OpenFAST)	Aerodynamic modeling (integrated with OpenFAST)	Dynamic stall, yaw, tower shadow effects, BEM integration	Yes (part of OpenFAST)
ANSYS Fluent	ANSYS Inc.	High-fidelity CFD simulation	3D flow analysis, turbulence modeling, structural-fluid coupling	No

UNCORRECTED PROOF

XFlow CFD	Dassault SystÃ¨mes	Lattice-Boltzmann CFD for unsteady aerodynamics	Mesh-free CFD, transient flow, ideal for complex geometries	No

In this study, QBlade was used as an open-source software for blade aerodynamics analysis. It is developed by TU Berlin and it enables wind turbine design and aerodynamic analysis using the BEM method, featuring a user-friendly interface and integration with XFOIL for airfoil generation and polar data computation [52]. In QBlade, simulations are organized around a modular hierarchy that reflects the core physical elements of a turbine system: aerodynamics, elasticity and hydrodynamics.

Researchers have employed QBlade extensively for aerodynamic evaluation of small and medium-scale turbines. For example, Kumar et al. used QBlade to analyze the aerodynamic behaviour of a small HAWT operating in low-wind-speed environments, where graphical relationship between power, tip-speed ratio, velocity and coefficient of pressure along aerofoil is shown [53]. Batu et al. applied QBlade to assess the aerodynamic performance of wind turbine blades made from natural fiber composites, investigating the material's mechanical performance [54]. In another study, Husaru et al. tested the effect of the value of the yaw angle on the global performances of HAWT [55]. Furthermore, Alaskari et al. employed QBlade for studying the effect of design parameters (twist angle and chord length) on the behaviour and performance of the wind turbine [56]. Moreover, for design optimization, platforms like MATLAB are often employed due to their flexibility and robust optimization toolboxes. MATLAB can be coupled with simulation tools like QBlade or OpenFAST to create automated design loops that vary geometric or aerodynamic parameters and evaluate performance [57]–[59].

Considering the limitations in North Macedonia regarding research on site-specific aerodynamic blade design, the primary objective of this study is to develop and comparatively evaluate alternative blade geometry formulations for a horizontal-axis wind turbine operating under the wind regime of a selected high-potential site in North Macedonia. Blade geometries are derived using four classical analytical methods (Ingram, Jamieson, Manwell et al., and Betz), together with an additional iterative BEM-based refinement aimed at obtaining a more realistic and manufacturable chord distribution.

The site is characterized by average wind speeds in the range from 6.0 to 7.5 m/s at an altitude of 420 m, corresponding to IEC Class III wind conditions. A HAWT with geometric and operating parameters representative of turbine suitable for such wind regimes was therefore considered. Airfoil profiles were evaluated based on both aerodynamic efficiency and structural requirements, and selected airfoils were used for the rotor blade design.

The resulting blade geometries, characterized by distinct chord and twist distributions, were implemented in QBlade to evaluate their aerodynamic performance under identical operating conditions. The analysis aims to identify the blade design approach that provides the most favourable balance between aerodynamic efficiency, loading characteristics, and geometric feasibility for wind turbines operating in moderate wind regimes.

MATERIALS AND METHODS

The aerodynamic analysis and rotor design in this study are based on the BEM approach, which combines momentum theory with blade element aerodynamics to estimate the performance of horizontal-axis wind turbines. Using this framework, the rotor geometry was determined through several blade design procedures based on airfoil aerodynamic characteristics and optimal operating conditions. The following subsections describe the theoretical background of the BEM method and the blade design procedure applied in this work.

UNCORRECTED PROOF

Blade Element Momentum Theory

Blade Element Momentum (BEM) Theory is a well-established method for calculating the forces acting on a wind turbine blade, i.e. the thrust force and the torque. Thrust in a wind turbine is the axial force exerted by the wind on the rotor blades and used for the turbine to generate power. The rotor also experiences a torque in the direction of rotation that opposes the torque that the generator exerts [60]. The BEM theory is based on a combination of a momentum balance on successive annuli of the rotor disk with a blade element representation of the sectional aerodynamics (Figure 2), i.e. the momentum theory and the blade element theory [61].

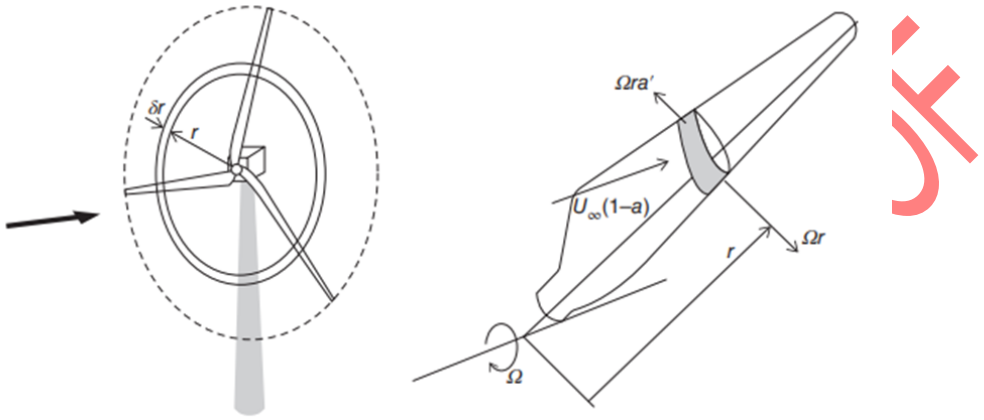

Figure 2. Schematic representation for BEM: rotor disc ring generated by blade element [61]

The momentum theory applies the conservation of linear and angular momentum to air flowing through the rotor disk, calculating the force and energy extracted from the wind. To allow variation of both induced velocity components, the analysis is based on the use of an annular stream tube of a rotor disc, with radius r and thickness dr, resulting in a cross-sectional area equal to $2\pi rdr$. Considering that the wind flow across the rotor is slowed down by the turbine, the fractional decrease in the velocity U at the rotor plane of a wind turbine relative to the free stream velocity U_∞ is defined by the axial induction factor a.

The change in axial momentum of air as it passes through the rotor results in thrust force N. Thus, the differential thrust dN is obtained by applying the conservation of linear momentum:

$$dN = \rho U_\infty^2 2a\,(1-a)\,2r\pi dr \tag{1}$$

The blades rotate with an angular velocity Ω about an axis normal to the rotor plane and parallel to the wind direction. The velocity at the rotor disc entrance does not have a rotational component unlike the flow behind the disc. The change in tangential velocity is expressed in terms of an angular induction factor a'. Immediately downstream of the disc, the tangential velocity of air is $2r\Omega a'$ and remains constant as air progresses down the wake, while in the plane of the disc the air tangential velocity is $r\Omega a'$.

The differential torque dQ imparted to the blades is found from the angular momentum conservation:

$$dQ = \rho U_\infty\,(1-a)\,2\Omega a' r^2 2\pi r dr \tag{2}$$

Thus, momentum theory results in two equations, (1) and (2), that define the thrust and torque on an annular section of the rotor as a function of the flow conditions.

The blade element theory calculates aerodynamic forces at every blade section based on the angle of attack, airfoil properties and local flow conditions. The lift L and drag D forces are perpendicular and parallel, respectively, to the relative wind velocity W that acts at an angle ϕ to the plane of rotation. For a turbine with B blades, the differential thrust and differential torque on the annular rotor section are expressed as:

UNCORRECTED PROOF

$$dN = \frac{1}{2} Bc\rho W^2 (C_L \cos\phi + C_D \sin\phi) dr \quad (3)$$

$$dQ = \frac{1}{2} Bc\rho W^2 (C_L \sin\phi - C_D \cos\phi) r dr \quad (4)$$

where C_L and C_D are lift and drag coefficient, respectively, at the blade section.

Thus, blade element theory results in two equations, (3) and (4), that define the thrust and torque at a blade section as a function of blade geometry**Error! Reference source not found.**.

Wind turbine performance. The total power P from the rotor is calculated summing contributions from each annulus by:

$$P = \int_{r_h}^{R} dP dr = \int_{r_h}^{R} \Omega dT dr \quad (5)$$

where r_h is the hub radius and R is the rotor radius.

The power coefficient C_p is given by:

$$C_p = \frac{P}{P_{wind}} = \frac{\int_{r_h}^{R} \Omega dT dr}{\frac{1}{2}\rho v^3 R^2 \pi} \quad (6)$$

Blade design

Airfoil shape. A wind turbine blade is a long, aerodynamically shaped structure attached to the rotor hub of a wind turbine. To maximise the wind turbine power output, it is necessary to obtain a suitable solution to the BEM equations for a given operating mode, resulting in an optimal blade design. An airfoil of a given shape generates a lift force L and drag force D, dependent on wind velocity, chord length c and angle of attack α. The aerodynamic lift force drives the turbine power production, making its maximization through appropriate design crucial whereas friction generates a resisting drag force that opposes blade motion and should be minimized.

The lift and drag coefficient C_L and C_D depend on the Reynolds number and the angle of attack (AoA). Reynolds number, which varies with wind speed, should be considered for selection of airfoils that perform well across the expected operating range [62]. The design angle of attack α_0 is the angle between the chord line of the blade section and the relative wind at which the airfoil has highest glide ratio, i.e. lift-to-drag ratio. Thus, an airfoil with a high glide ratio should be selected for rotor blade design to ensure aerodynamic efficiency:

Usually, the blade is designed using a thin airfoil for obtaining high glide ratio at the tip while the root region is designed using a thicker airfoil for structural support. This can be achieved by using different airfoils and appropriate chord and twist angle distribution along the blade length.

Chord length distribution and twist angle distribution. To determine the cross-sectional shape distribution on the blade, a number of design parameters are required to satisfy the requirements of the BEM theory equation such as: tip-speed-ratio λ, desired number of blades B, the radius of the blade R and airfoil for which its aerodynamic characteristics are known as a function of AoA, i.e. C_L, $C_D=f(\alpha)$.

The tip-speed ratio (TSR) is a dimensionless number that represents the ratio between the speed of the blade tip and the speed of the incoming wind:

$$\lambda = \frac{\Omega R}{U_\infty} \quad (7)$$

UNCORRECTED PROOF

The chord length c is a straight line connecting the leading and the trailing edge of the airfoil section. Chord length distribution describes how this length changes from root to tip of the turbine blade. Larger chord is required near the blade root to handle torque and bending loads. Smaller chord is necessary toward the blade tip to reduce drag and weight.

The relative wind angle ϕ changes with radius, so the blade must be twisted to maintain a near-optimal AoA [62]. The angle between the chord line of a blade section and the rotor plane is called a twist angle θ. The following relation can be derived:

$$\phi = \theta + \alpha_0 \tag{8}$$

The twist angle distribution describes how this angle varies along the blade span, from root to tip. A wind turbine blade is typically composed of multiple airfoil sections joined together with a varying twist angle, ending in a circular flange at the root. HAWTs often have a twist at the tip close to zero.

Jamieson [63] offers an equation for the optimum chord distribution of a blade given an airfoil with maximum glide ratio and lift coefficient at the corresponding design AoA.:

$$c(r) = \frac{16\pi R^2}{9BC_L\lambda^2 r} \tag{9}$$

Neglecting the drag force and the tip losses, Betz [64] presents the chord distribution by the following expression:

$$c(r) = \frac{16\pi R}{9BC_L\lambda\sqrt{\lambda_r^2 + \frac{4}{9}}} \tag{10}$$

For both Jamieson and Betz models, an optimal blade twist distribution is determined from the inflow angle ϕ:

$$\phi(r) = tan^{-1}(\frac{2}{3\lambda_r}) \tag{11}$$

Ingram [65] gives a linear distribution of chord length and a twist angle distribution based on an ideal rotor blade shape derived with wake rotation, zero drag and zero tip losses:

$$c(r) = \frac{8\pi r \sin\phi}{3B\lambda_r} \tag{12}$$

Durran [66], Manwell et al. [9] also give equations for chord length and twist angle distribution of a turbine blade for an ideal rotor that includes the effects of wake rotation but ignores drag and tip losses, for a previously selected design AoA for which the airfoil glide ratio is highest:

$$c(r) = \frac{8\pi r(1 - cos\,\phi)}{BC_l} \tag{13}$$

For both Ingram and Manwell models, the blade twist distribution is defined from the inflow angle ϕ:

$$\phi(r) = \frac{2}{3}tan^{-1}\left(\frac{1}{\lambda_r}\right) \tag{14}$$

In addition to the classical analytical formulations, an iterative blade design approach based on BEM theory was implemented. The iterative procedure determines the chord and twist distributions through successive updates of the local aerodynamic conditions along the blade span.

For each radial blade element, initial estimates of the axial induction factor a, and tangential induction factor a' are assumed. Using these values, the local inflow angle ϕ is calculated as:

$$\phi(r) = \tan^{-1}\left(\frac{(1-a)V}{(1+a')\Omega r}\right) \tag{15}$$

UNCORRECTED PROOF

From the selected design angle of attack and the corresponding airfoil characteristics, the lift and drag coefficients are obtained and used to calculate the normal and tangential force coefficients. These values allow the local blade solidity and chord length to be determined. The local solidity σ is defined as:

$$\sigma = \frac{Bc}{2\pi r} \tag{16}$$

The induction factors a and a' are subsequently updated using the BEM momentum equations, and the procedure is repeated until convergence is achieved. Once convergence is reached for each radial station, the corresponding chord and twist distributions are obtained along the blade span. A minimum tip chord constraint was applied to ensure geometric feasibility and manufacturability of the blade.

MODEL PARAMETERS

This section presents the main parameters used for the wind turbine model considered. The operating conditions and principal geometric characteristics of the reference turbine are first introduced. In addition, the airfoil families investigated for the blade design are described.

Main operating and geometric parameters of the wind turbine

This research studies the aerodynamic performance of three alternative wind turbine blade designs, evaluated within the operational parameters of the VESTAS V110-2.0 MW wind turbine. The observed location in North Macedonia is characterized by a 420 m height above sea level and wind speed range between 6 and 7.5 m/s. According to [67], the designated wind speed range aligns with IEC Wind Class III, from which the VESTAS V110-2.0 MW turbine was consequently selected for the analysis. The primary objective is to analyse and compare the behaviour of different blade designs under identical operating conditions derived from the V110-2.0 MW configuration. A tip-speed ratio TSR=7 was selected in the design point.

The VESTAS V110 wind turbine features a rotor diameter of D=110 m, rotor radius of R=55 m and operates with a hub radius of r_h=1 m. Its rated power is 2.0 MW at a rated wind speed of 11.5 m/s. The cut-in and cut-out speed are 3 m/s and 20 m/s, respectively. The main dimensions of this HAWT are shown in Figure 3.

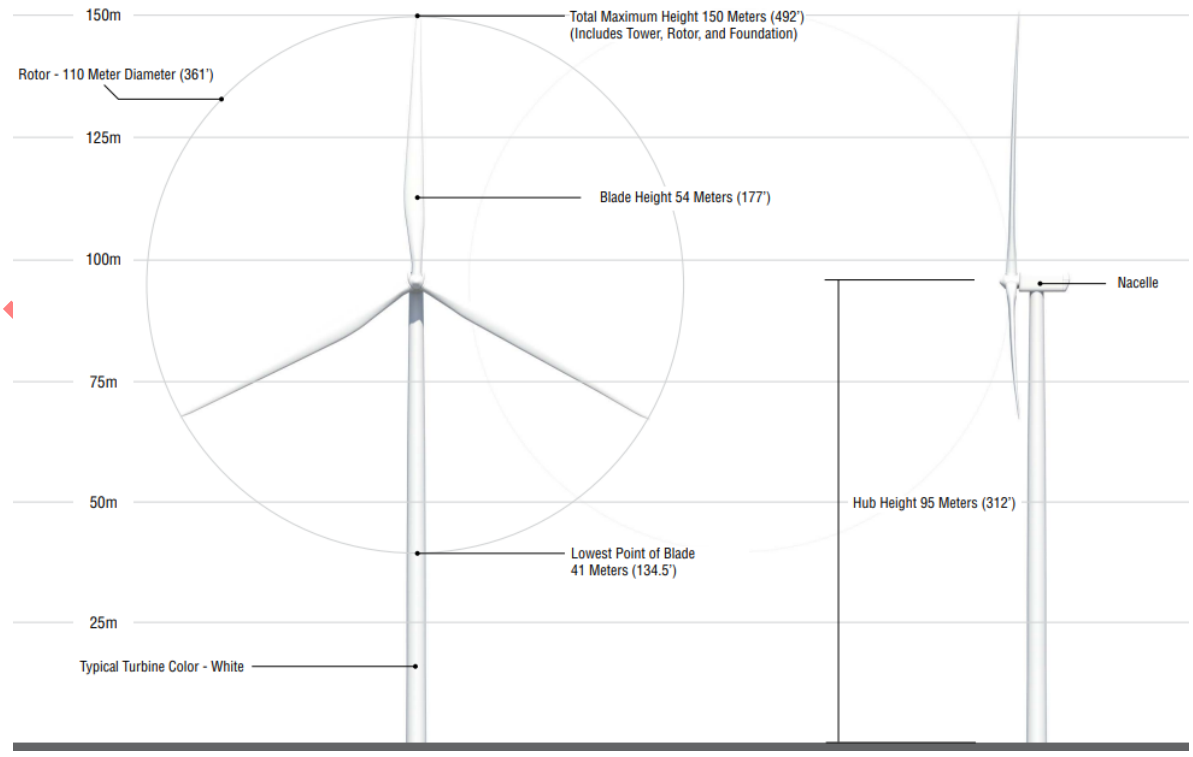

REJECTED PROOF

Figure 3. HAWT main dimensions [67]

Investigated airfoils

In the 1980s and early 1990s, wind turbine blades were commonly designed using existing aeronautical airfoils such as the NACA 44 and NACA 63 series, with increased thickness obtained by geometric scaling. However, wind tunnel tests and calculations showed that thicker NACA profiles suffered significant performance degradation (increased drag, and reduced Cl,max) due to premature transition and early separation. These limitations motivated the development of dedicated wind-turbine airfoil families in the United States and Europe.

To improve performance across the thickness range required in wind turbine blades, the FFA-W3 series was developed from the earlier FFA-W1 profiles with increased aft loading and adjusted camber. Designed specifically for pitch-regulated turbines, FFA-W3 family includes airfoils with moderate to high thickness ratios (up to 36% thickness) provide improved lift and greater robustness under realistic operating conditions, with a moderate increase in pitching moment [35]. Among other, FFA-W3 airfoils are used along the blade span of the DTU 10 MW reference wind turbine [68] and the IEA Wind 15-Megawatt Offshore Reference Wind Turbine [69]. In accordance with these characteristics, FFA-W3 profiles were selected along the aerodynamically active portion of the blade span in this study.

Airfoils from the Delft University (DU) family have been widely applied in MW-scale wind turbine blade design. For example, the NREL 5 MW reference turbine employs DU-series airfoils with thicknesses ranging from 21% to 40% in the inboard and mid-span regions [70]. During the second half of the 1990s, increased understanding of wind turbine noise mechanisms and rotational effects led to the development of updated DU airfoils optimised for specific radial positions. In this context, an 18% thick tip airfoil with relatively low maximum lift (DU 95-W-180) and a 30% thick inboard airfoil (DU 97-W-300) were developed as baseline profiles for outer and inner blade regions, respectively [37].

RESULTS AND DISUCSSION

This section presents the results of the airfoils aerodynamic analysis and the performance simulations of the investigated wind turbine blade designs. The results are subsequently discussed and compared in order to assess the relative performance of the blade designs and their potential practical applicability.

Airfoil evaluation and selection

DU 97-W-300 was specifically developed for inner blade regions (~40% span) of MW-scale turbines, targeting a maximum lift coefficient of 1.5–1.6 at high Reynolds numbers. The 30% thickness and thick trailing edge provide structural suitability while maintaining acceptable roughness performance. Accordingly, DU 97-W-300 was selected for the inboard region (20-35% radial span) of the present blade, where sufficient structural thickness, robust roughness performance, and controlled stall characteristics are required.

The mid-span region of the blade contributes substantially to rotor torque and consequently to overall power production, while also operating at high relative velocities, requiring an airfoil that provides both structural stiffness and high aerodynamic efficiency. The FFA-W3-241 airfoil is employed in this region, extending from 35–75% of the radial position, as it maintains a favourable lift-to-drag ratio within the operating range, while its 24% thickness ensures sufficient structural stiffness.

FFA-W3-211 airfoil is widely used in the wind energy community as part of IEA reference wind turbine designs, especially as a tip aifoil [71]. Thus, FFA-W3-211 was adopted in the outboard blade region to prioritise aerodynamic efficiency and reduced tip-loss sensitivity. The thinner section (21% thickness-to-chord ratio) lowers drag, and delays separation compared to

UNCORRECTED PROOF

thicker profiles, which is important in the high-velocity tip region. At the same time, it provides sufficient lift and predictable stall behaviour for preventing sudden load variations [72].

The selected airfoils shapes are shown in Figure 4Figure 3.

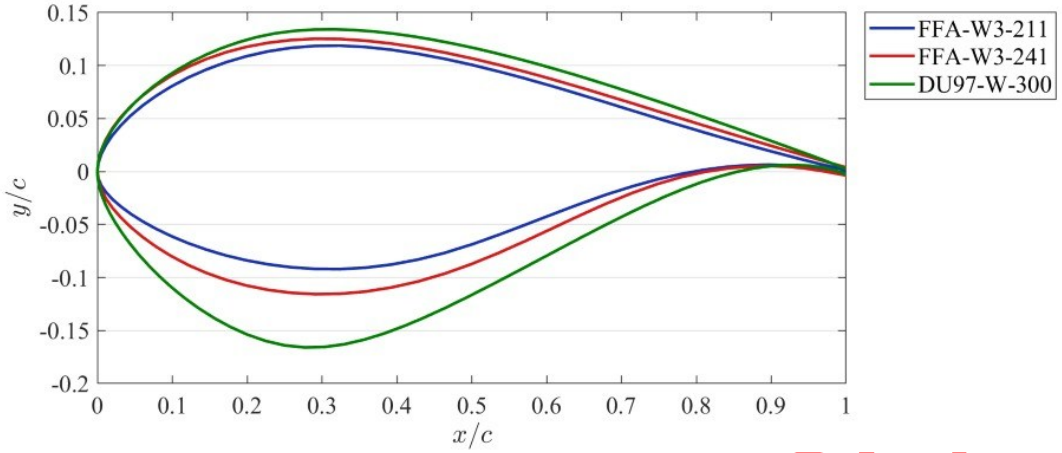

Figure 4. Shapes of selected airfoils for wind turbine blade design represented by their upper and lower contour

In practical large-scale wind turbine applications, Reynolds number varies along the blade span, potentially modifying lift, drag, and stall characteristics compared to single Reynolds number evaluations. Thus, preliminary testing and computational simulations were performed with the objective of determining the aerodynamic coefficients of the selected airfoils at different wind conditions. Typical Reynolds numbers relevant to flow around wind turbine blades are of the order of 10^6 to 10^7 [61]. Accordingly, airfoil aerodynamic characteristics were evaluated at Reynolds numbers of $3 \cdot 10^6$, $6 \cdot 10^6$, and $9 \cdot 10^6$, representing conditions within this operational range. Figure 5, Figure 6, and Figure 7 illustrate the variation of the lift coefficient (C_l) and drag coefficient (C_d) as functions of the AoA for the DU-97-W-300, FFA-W3-241 and FFA-W3-211.

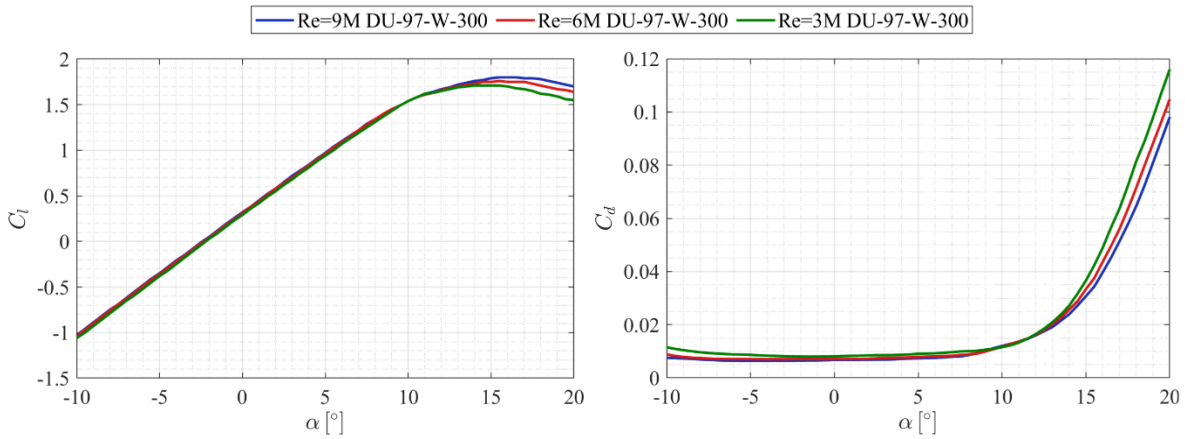

a) b)

Figure 5. Aerodynamic coefficients dependency of DU-97-W-300 on AoA at different Reynolds numbers: a) lift and b) drag coefficient

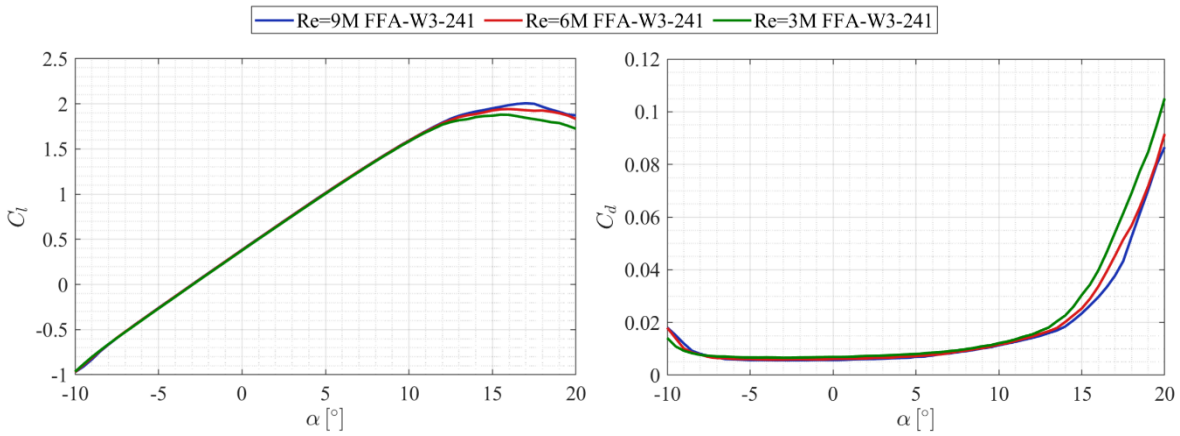

a) b)

Figure 6. Aerodynamic coefficients dependency of FFA-W3-241 on AoA at different Reynolds numbers: a) lift and b) drag coefficient

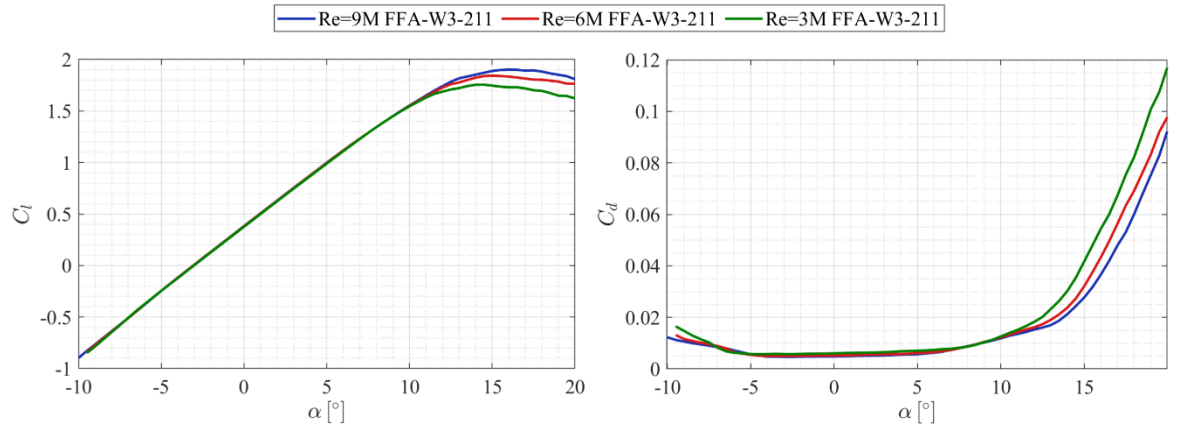

a) b)

Figure 7. Aerodynamic coefficients dependency of FFA-W3-211 on AoA at different Reynolds numbers: a) lift and b) drag coefficient

Across the investigated Reynolds-number range ($3 \cdot 10^6$ - $9 \cdot 10^6$), all three airfoils exhibit limited sensitivity in the attached-flow region, as the lift coefficient curves largely coincide up to approximately 10–12°, indicating stable lift behaviour within the normal operating range. Differences become more evident near stall. For all profiles, increasing Reynolds number produces a modest rise in $C_{L,max}$ and a slight delay in stall onset, while lower Reynolds numbers lead to earlier lift degradation and steeper drag growth beyond 12–14° due to earlier separation. The Reynolds sensitivity is most pronounced for the thinner FFA-W3-211, moderate for the FFA-W3-241, and least for the thicker DU 97-W-300, reflecting the increased boundary-layer robustness of thicker sections.

Overall, the results indicate that Reynolds-number effects are modest within the operational angle-of-attack range but become increasingly relevant near stall. Since wind turbine blades frequently operate under stalled conditions, the absence of reliable aerodynamic data at high angles of attack can present a limitation. Thus, polar extrapolation at 360° angle was performed using the Viterna method [73], a well-established empirical approach for extrapolating airfoil lift and drag into deep stall, specifically developed for wind turbines, validated using measured data and widely used in modern wind turbine aerodynamic models.

To account for the spanwise and operational variation in Reynolds number, a multi-polar approach was used. Airfoil polars were generated at several Reynolds numbers in the range of

$1 \cdot 10^6$-$11 \cdot 10^6$ and interpolated during BEM simulations, ensuring that lift and drag characteristics reflect the local flow conditions.

The airfoil design AoA selection in this study was primarily guided by aerodynamic performance indicators under representative Reynolds number conditions. For further assessment, the relationship between the glide ratio (C_L/C_D) and the angle of attack (α) was analysed for several Reynolds numbers. The airfoils exhibit their maximum glide ratio at approximately α=7°, corresponding to a lift coefficient of about $C_L \approx 1.2$. Accordingly, these values were adopted as the design angle of attack and design lift coefficient for the blade design.

The blades were modelled using Qblade software for each of the methods. To design the rotor blade based on BEM theory, the blade with length of 54 m (rotor radius R=55 m) was divided into twenty elements and the calculated chord (c) and twist angle (θ) distributions were inserted. The blade was twisted in such way that the angle of attack (α) remained constant at all sections. The distributions of the chord length and twist angle using (9)-(14) are presented in Figure 8.

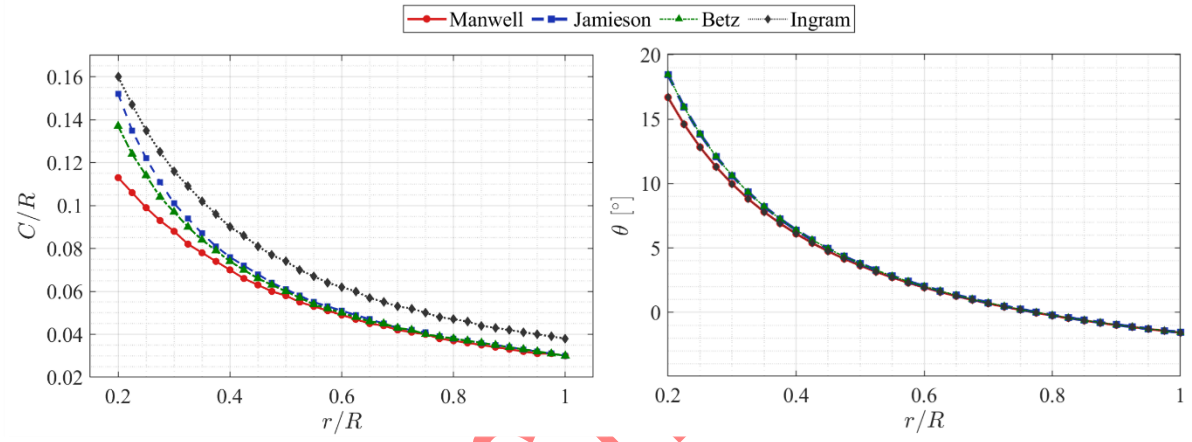

Figure 8. Distribution of blade geometry parameters along the rotor span: a) chord length distribution, showing the variation in blade width from root to tip; (b) twist angle distribution, illustrating the change in blade pitch to maintain optimal angle of attack across the span

The chord and twist distributions obtained from the four design methods show the expected variation along the blade span. In all cases, the chord is largest in the inboard region and gradually decreases toward the tip, while the twist angle decreases from higher values near the root toward values close to zero at the blade tip in order to maintain an appropriate angle of attack along the blade. Among the considered formulations, the Ingram method produces the largest chord values along most of the span, indicating the highest blade solidity, followed by the Jamieson method. The Betz method yields intermediate chord values, whereas the Manwell method results in the smallest chord distribution. With respect to the twist distribution, the Jamieson and the Betz formulation predict slightly higher twist angles in the inner blade region, while all methods produce very similar twist trends along the blade span. In addition, a rotor blade was designed with the application of an iterative blade BEM approach.

According to these distributions, the shapes of selected blades are given in Figure 9 where their design specifications and characteristics are visually illustrated for comparison.

UNCORRECTED PROOF

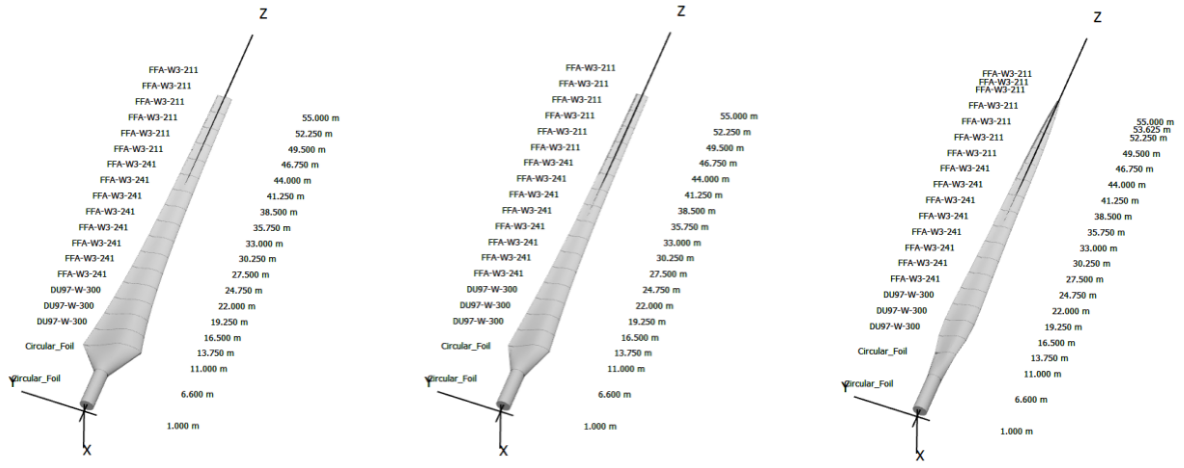

a) b) c)

Figure 9. HAWT blade design generated in Qblade software by applying the methods for calculating wind turbine blade geometry parameters of: a) Ingram; b) Manwell et al.; c) Iterative BEM

Performance simulation results

Cp-TSR curve. Figure 10 illustrates the aerodynamic performance of the four distinct wind turbine blade designs by plotting the power coefficient (C_p) as a function of the tip-speed ratio TSR. Each curve demonstrates the characteristic blade design, where the power coefficient primarily increases with TSR, reaches a peak and then declines as TSR continues to rise. This trend appears due to the physical interaction between aerodynamic forces - at low TSR values, blades rotate too slowly to effectively extract wind energy, while at high TSR values, drag forces and flow separation begin to dominate. Peak C_p identifies the optimal operating point for each design, indicating the TSR at which maximum energy extraction from the wind is achieved.

Among the classical formulations, the Manwell method predicts the highest maximum power coefficient of C_p=0.476 at TSR≈7. The Jamieson and Betz methods produce nearly identical curves, reaching peak values of approximately C_p=0.47 at TSR≈6.9, which corresponds to only about 1.3% lower efficiency compared to Manwell. In contrast, the Ingram formulation results in a slightly lower peak value of C_p≈0.46, representing a 3.4% reduction relative to Manwell, and reaches its maximum at a lower TSR of about 5.4.

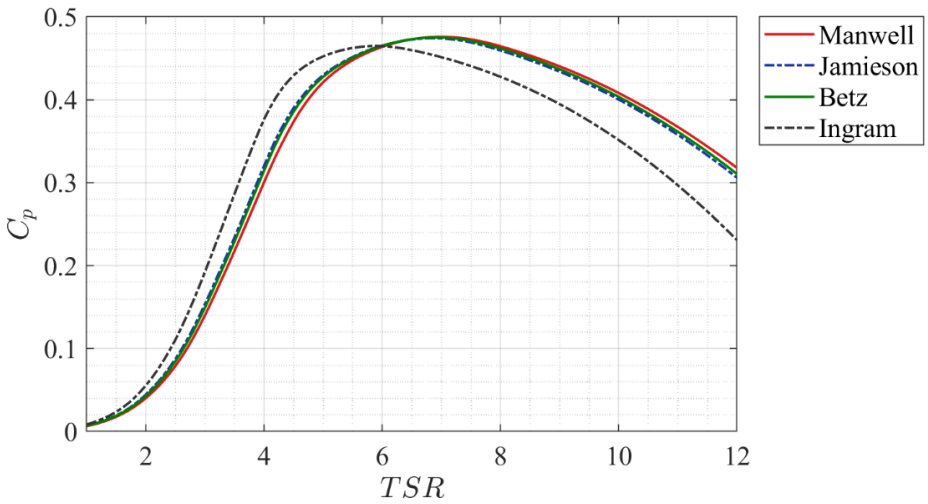

Figure 10. Power coefficient (C_p) as a function of tip-speed ratio (TSR) for various rotor blade designs, illustrating the aerodynamic efficiency of each blade across a range of TSR values

CORRECTED PROOF

The Manwell curve reaches its maximum power coefficient at the design tip-speed ratio (TSR≈7), indicating that the rotor performs optimally at the intended operating condition defined during the design process. In contrast, the Ingram curve is shifted toward lower TSR values, with the maximum C_p occurring around TSR≈5.4, which suggests that this formulation predicts the optimal aerodynamic loading at a lower rotational speed relative to the design TSR.

Although the classical analytical methods predict very similar aerodynamic performance, the resulting blade geometries exhibit relatively large chord values, compared to the maximum chord value of the VESTAS blade. Moreover, large values in the root region increase blade mass and consequently raise manufacturing cost and structural complexity. To obtain a more realistic blade geometry, an iterative blade BEM approach was applied. Figure 11 shows the power coefficient C_p and thrust coefficient C_t variation in terms of TSR for the blade designs obtained with the Ingram, Manwell and iterative BEM models.

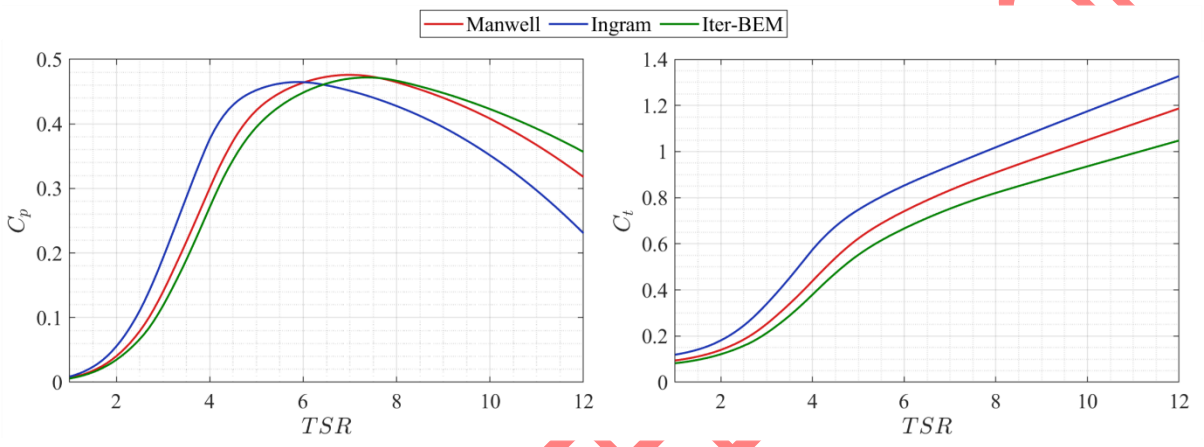

Figure 11. Power coefficient (C_p) and thrust coefficient (C_t) as a function of tip-speed ratio (TSR) for selected rorot blade designs

The iterative design achieves a very similar peak C_p value of about 0.472 at TSR ≈ 7.2–7.3, representing a reduction of less than 1% relative to Manwell, while maintaining nearly identical curve shape and operating region.

More pronounced differences are observed in the thrust coefficient (C_t) behaviour. For the Manwell design, the thrust coefficient increases steadily with TSR, reaching $C_t \approx 0.83$ at TSR=7. The Ingram formulation produces consistently higher thrust coefficients across the entire TSR range, reaching approximately C_t≈0.94 at TSR=7, which is about 13% higher than Manwell. This indicates a substantially higher aerodynamic loading of the rotor. In contrast, the iterative design yields the lowest thrust coefficients, with C_t≈0.75 at TSR=7, corresponding to a reduction of approximately 10% compared to Manwell and about 20% compared to the Ingram design. The overall C_t–TSR curve for the iterative blade therefore remains significantly below the classical formulations throughout the operating range.

P-V_w curve. Power curves show the relationship between wind speed and turbine power depicting the wind turbine operating range. Figure 12 presents the power curve corresponding to the blade designs compared to the original power curve of VESTAS.

The predicted power curves of the analytically designed rotors closely match the reference curve of the Vestas V110-2 MW turbine. This agreement indicates that the selected aerodynamic parameters and rotor design assumptions are consistent with industrial-scale turbine performance. Minor deviations near the rated region are mainly associated with simplified control modelling in the BEM simulations.

UNCORRECTED PROOF

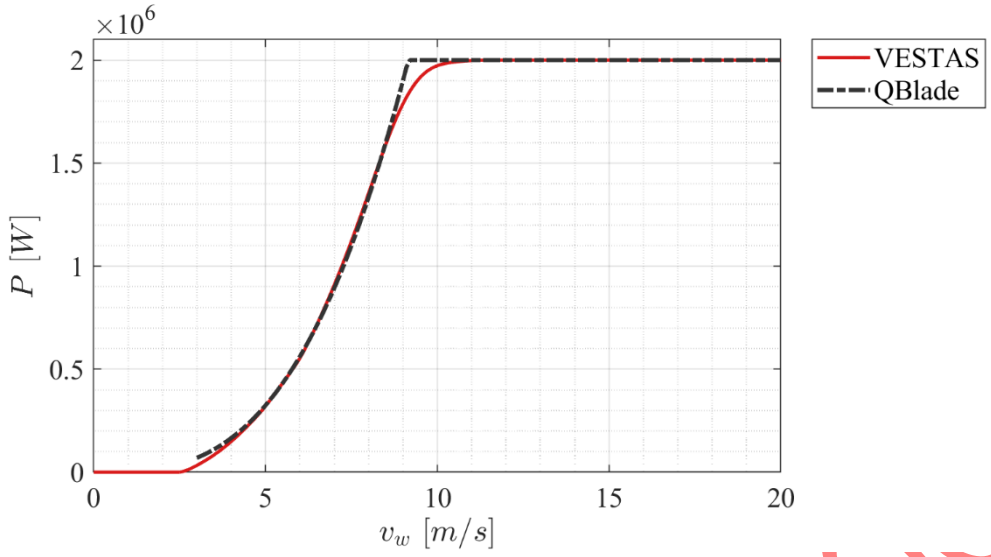

Figure 12. HAWT power curves for the blade designs from Qblade and from the reference VESTAS turbine representing the turbine power output as a function of wind speed to depict turbine performance across its operational range

No power is produced when the wind speed is below the cut-in value. As the wind speed increases, the turbine enters the power-producing region and the power increases rapidly with wind speed. This increase follows approximately a cubic trend, since the available wind power is proportional to v_w^3. In the region between roughly 4 and 9 m/s, the turbine operates in the aerodynamic control region where the rotor extracts as much energy as possible from the wind. At around 9 m/s (Qblade) and 11.5 m/s (original curve) the turbine reaches its rated power of 2 MW, after which the power remains constant despite further increases in wind speed till reaching the cut-out speed at which the turbine stops to protect the blades in strong winds. The rated power of 2 MW indicates the maximum power output maintained by the control system under high wind conditions.

The reason the power curves of all blades designs are identical and presented as one power curve obtained from Qblade is that the rated power and control strategy are the same for all designs. Even though the blade geometries differ slightly, their aerodynamic performance (as seen in the C_p –TSR curves) is very similar, with almost the same maximum C_p. As a result, the differences between the blade designs do not appear clearly in the power curve, which is why the curves overlap almost completely.

C_p-V_w curve. The correlation between the power coefficient and the wind speed for different models is given in Figure 13.

It can be observed that Manwell and Iter-BEM designs achieve slightly higher C_p values, approaching about 0.47–0.48, while the Ingram formulation yields slightly lower values around 0.45. This indicates a marginally higher aerodynamic efficiency for the blades of Manwell and iterative BEM models under low wind conditions. Beyond the rated wind speed, the C_p values decrease rapidly for all designs as turbine power regulation becomes dominant. In this region the curves converge and show nearly identical behaviour, indicating that differences between the blade formulations primarily affect performance in the sub-rated operating regime, while their high-wind behaviour remains similar. Notably, the wind speed range corresponding to the IEC Class III regime considered in this study (6–7.5 m/s) lies within the region where the turbine operates close to its maximum aerodynamic efficiency, indicating that the evaluated blade designs are well suited for the local wind conditions.

UNCORRECTED PROOF

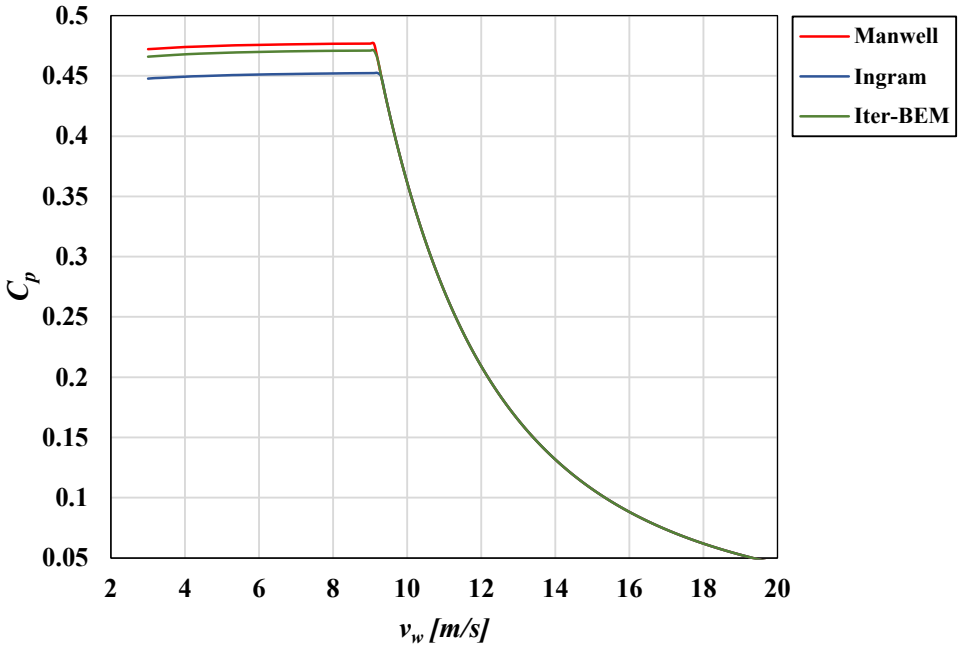

Figure 13. Power coefficient (C_p) as a function of wind speed, showing wind turbine aerodynamic efficiency across its operating range

C_q -TSR curve. Figure 14 is centred on torque coefficient C_q as a function of the tip-speed ratio for the three analysed designs.

The Ingram formulation produces the highest torque coefficient, reaching approximately C_q≈0.095 at TSR≈4–4.5, while the Manwell design gives intermediate values and the iterative BEM refinement results in the lowest peak torque coefficient. This behaviour reflects the higher blade solidity associated with the Ingram design, which increases aerodynamic loading and torque generation. In contrast, the iterative blade geometry produces slightly lower torque values, indicating reduced aerodynamic loading while maintaining comparable power performance.

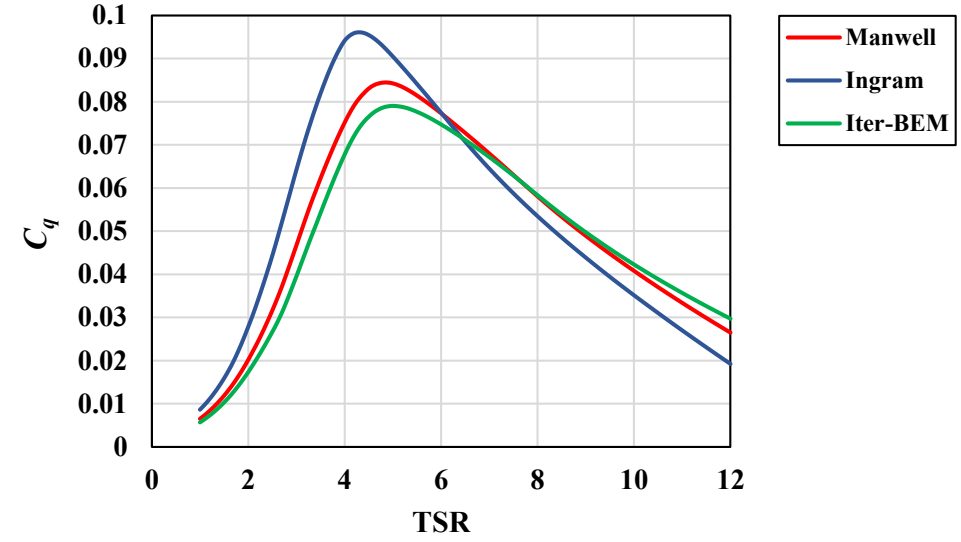

Figure 14. Torque coefficient as a function of tip-speed ratio (TSR) for different rotor blade designs showing how torque varies with rotor speed relative to wind speed

Therefore, although the Ingram formulation provides the highest torque generation, the Iter-BEM and Manwell designs may offer more balanced operational characteristics with reduced aerodynamic loading and improved geometric feasibility.

Discussion

The C_p curves show that all three designs maintain high aerodynamic efficiency over a relatively broad TSR range, with the Manwell and Iter-BEM formulations reaching peak values close to 0.47, while the Ingram design remains slightly lower. Since the dominant wind speeds at the selected site (6–7.5 m/s) fall within the region of near-maximum efficiency, only minor differences in Annual Energy Production (AEP) are expected among the examined blade geometries. This also suggests that turbine performance is not highly sensitive to moderate wind-speed variations within the typical operating range of the site. However, the C_q and C_t curves reveal clearer differences in aerodynamic loading. The Ingram design produces the highest torque and thrust coefficients, indicating increased loading and therefore potentially higher structural demands on the blade, hub, and drivetrain. In contrast, the Iter-BEM design maintains a C_p value very close to that of the Manwell design while yielding lower C_q and C_t values, suggesting reduced mechanical loading.

Based on the site-specific wind-speed time series, the estimated Annual Energy Production (AEP) is approximately 8.5 GWh/year. This value is somewhat higher than the AEP indicated by the manufacturer's reference curve (≈6.7 GWh/year) for the same average wind speed of 6.5 m/s. The difference can be attributed to the use of measured 10-minute wind-speed data in the present study, whereas the manufacturer curve is derived from a reference Weibull distribution based on generalized wind conditions. Consequently, the calculated value reflects the actual wind-speed frequency distribution at the analysed site.

From a practical perspective, these results highlight an important design trade-off between marginal gains in aerodynamic performance and structural or manufacturing complexity. In particular, designs predicting larger root chord dimensions, such as the Ingram formulation, may introduce manufacturing challenges due to increased blade mass and thicker structural laminates required in the inboard region. The smoother and more moderate chord distribution obtained with the Iter-BEM approach reduces excessive chord dimensions near the blade root, which may simplify fabrication and limit material requirements while maintaining comparable energy capture. For wind resource conditions typical of IEC Class III sites such as the analysed location in North Macedonia, this indicates that modest geometric refinements can preserve aerodynamic efficiency while improving geometric feasibility.

In practical implementations, blades of this size are typically manufactured using glass-fibre reinforced polymer (GFRP) composites with multiaxial E-glass reinforcements and sandwich core materials, which provide a favourable stiffness-to-weight ratio and sufficient fatigue resistance to withstand aerodynamic and cyclic loads in modern utility-scale wind turbines [74]–[76].

Although the analysis was conducted for a specific high-potential site, the proposed blade design methodology can be applied to other wind locations by adapting the input wind characteristics. In such cases, the chord and twist distributions would be recalculated according to the local wind regime and associated aerodynamic loading conditions. Consequently, the presented methodology provides a practical framework for evaluating blade configurations adapted to local wind conditions prior to more detailed structural or cost optimisation and may support more informed turbine design decisions for future wind energy deployment in the region.

CONCLUSIONS

In North Macedonia, only a part of the available wind energy is used, and there are regions with significant potential. However, to the authors knowledge, no research studies exist that investigate a rotor blade design for wind turbine blade for this site. In this regard, research was conducted to increase the efficiency of a HAWT for one suitable location in the country for wind farms construction.

UNCORRECTED PROOF

A numerical model was developed using Qblade software based on BEM theory. The model configuration is based on the operating and fundamental geometric parameters of a commercially available HAWT selected to correspond to the wind speed range found at the specific site, the air density calculated for the site altitude and the desired installed capacity. Multiple aerodynamic blade profiles were numerically analysed. Following the performance evaluation of these airfoils, three were selected based on their aerodynamic efficiency and structural performance to be used in the rotor blade design. Three rotor blade models were then developed, with different chord length and twist angle distributions according to methods found in literature, specifically the models of Jamieson, Ingram, Manwell et.al, and Betz. A numerical simulation model of airflow over blades with different geometries was created to analyse their influence on HAWT performance across a wide wind speed range. The simulations provided performance indicators of the turbine among which power coefficient, thrust coefficient, and torque coefficient.

The comparative analysis showed that the examined blade formulations provide very similar aerodynamic efficiency, with peak power coefficients close to $C_p \approx 0.47$. However, the designs differ in their predicted aerodynamic loading and geometric characteristics. While the Betz, Jamieson, and Manwell approaches lead to similar chord and twist distributions, the Ingram formulation produces larger chord values and higher loading coefficients. In contrast, the iterative BEM refinement yields a smoother and more moderate chord distribution while maintaining nearly the same aerodynamic performance.

The results indicate that iterative refinement of classical BEM formulations can support the development of blade geometries that balance aerodynamic efficiency with improved manufacturability and reduced mechanical loading. For wind conditions typical of IEC Class III sites such as the analysed location, moderate refinements of the obtained chord and twist distributions can preserve energy capture while improving geometric feasibility.

Although the analysis was conducted for a single site, the proposed design procedure can be applied to other wind locations by adapting the wind input data and operating conditions. Therefore, the presented approach provides a useful preliminary framework for evaluating blade configurations adapted to site-specific wind regimes.

ACKNOLEDGEMENT

This study is part of the project “Investigation of blade design through numerical and experimental methods for enhanced wind turbine performance”, supported and funded by Ss. Cyril and Methodius University in Skopje, through the University's Science and Research Fund.

REFERENCES

1. W. Fedak, S. Anweiler, R. Ulbrich, and B. Jarosz, “The concept of autonomous power supply system fed with renewable energy sources,” *Journal of Sustainable Development of Energy, Water and Environment Systems*, vol. 5, no. 4, pp. 579–589, Mar. 2017, https://doi.org/10.13044/j.sdewes.d5.0160.
2. Q. Hassan, P. Viktor, T. J. Al-Musawi, B. M. Ali, S. Algburi, H. M. Alzoubi, A. K. Al-Jiboory, A. Z. Sameen, H. M. Salman, and M. Jaszczur, “The renewable energy role in the global energy Transformations,” *Renewable Energy Focus*, vol. 48, p. 100545, 2024, https://doi.org/https://doi.org/10.1016/j.ref.2024.100545.
3. R. Weiss, “Decarbonised district heat, electricity and synthetic renewable gas in wind- and solar-based district energy systems,” *Journal of Sustainable Development of Energy, Water and Environment Systems*, vol. 9, no. 2, 2021, https://doi.org/10.13044/j.sdewes.d8.0340.

UNCORRECTED PROOF

4. International Energy Agency (IEA), "Global Energy and Climate Model," Nov. 12, 2025. https://www.iea.org/reports/global-energy-and-climate-model (accessed Mar. 07, 2026).
5. E. T. Sayed, A. G. Olabi, A. H. Alami, A. Radwan, A. Mdallal, A. Rezk, and M. A. Abdelkareem, "Renewable Energy and Energy Storage Systems," *Energies*, vol. 16, no. 3. MDPI, Mar. 2023, https://doi.org/10.3390/en16031415.
6. T. A. Hamed and A. Alshare, "Environmental Impact of Solar and Wind energy-A Review," *Journal of Sustainable Development of Energy, Water and Environment Systems*, vol. 10, no. 2, Mar. 2022, https://doi.org/10.13044/j.sdewes.d9.0387.
7. M. A. Hannan, A. Q. Al-Shetwi, M. S. Mollik, P. J. Ker, M. Mannan, M. Mansor, H. M. K. Al-Masri, and T. M. I. Mahlia, "Wind Energy Conversions, Controls, and Applications: A Review for Sustainable Technologies and Directions," *Sustainability*, vol. 15, no. 5. MDPI, Mar. 2023, https://doi.org/10.3390/su15053986.
8. C. Wulf and P. Zapp, "Sustainability assessment of innovative energy technologies – Hydrogen from wind power as a fuel for mobility applications," *Journal of Sustainable Development of Energy, Water and Environment Systems*, vol. 9, no. 3, 2021, https://doi.org/10.13044/j.sdewes.d8.0371.
9. J. F. Manwell, J. G. McGowan, and A. L. Rogers, *Wind Energy Explained: Theory, Design and Application*, 2nd Edition. Chichester, UK: John Wiley & Sons, 2009.
10. A. Chatzipanagi, A. Jaeger-Waldau, C. Cleret De Langavant, J. Gea Bermudez, S. Letout, A. Mountraki, A. Schmitz, A. Georgakaki, E. Ince, A. Kuokkanen, and D. Shtjefni, "Clean Energy Technology Observatory, Photovoltaics in the European Union – Status report on technology development, trends, value chains and markets – 2023," Luxembourg, 2023. https://doi.org/doi:10.2760/732675.
11. S. L. Dolan and G. A. Heath, "Life Cycle Greenhouse Gas Emissions of Utility-Scale Wind Power: Systematic Review and Harmonization," *J. Ind. Ecol.*, vol. 16, no. SUPPL.1, Mar. 2012, https://doi.org/10.1111/j.1530-9290.2012.00464.x.
12. IRENA, "World Energy Transitions Outlook 2022." https://www.irena.org/Digital-Report/World-Energy-Transitions-Outlook-2022 (accessed Mar. 07, 2026).
13. Research Center for Energy and Sustainable Development of the Macedonian Academy of Sciences and Arts (ICEOR MANU), "Faster toward a renewable future: using degraded and unusable land areas as sites for solar and wind power plants in North Macedonia," Skopje, North Macedonia, 2023.
14. A. A. Firoozi, F. Hejazi, and A. A. Firoozi, "Advancing Wind Energy Efficiency: A Systematic Review of Aerodynamic Optimization in Wind Turbine Blade Design," *Energies* , vol. 17, no. 12, p. 2919, Mar. 2024, https://doi.org/10.3390/en17122919.
15. S. El Mouhsine, K. Oukassou, M. M. Ichenial, B. Kharbouch, and A. Hajraoui, "Aerodynamics and structural analysis of wind turbine blade," *Procedia Manuf.*, vol. 22, pp. 747–756, 2018, https://doi.org/https://doi.org/10.1016/j.promfg.2018.03.107.
16. K. Yang, "Geometry design optimization of a wind turbine blade considering effects on aerodynamic performance by linearization," *Energies (Basel).*, vol. 13, no. 9, p. 2320, Mar. 2020, https://doi.org/10.3390/en13092320.
17. L. Pinelli, A. Amedei, E. Meli, F. Vanti, B. Romani, G. Benvenuti, M. Fabbrini, N. Morganti, A. Rindi, and A. Arnone, "Innovative Design, Structural Optimization, and Additive Manufacturing of New-Generation Turbine Blades," *J. Turbomach.*, vol. 144, no. 1, Mar. 2021, https://doi.org/10.1115/1.4051936.
18. V. K. Venkateswaran, U. Fernandez-Gamiz, K. Portal-Porras, and J. Ilzarbe, "Numerical study on aerodynamics of small scale horizontal axis wind turbine with Weibull analysis," *Sci. Rep.*, vol. 14, 2024, https://doi.org/10.1038/s41598-024-78503-2.
19. L. Thomas and M. Ramachandra, "Advanced materials for wind turbine blade- A Review," *Mater. Today Proc.*, vol. 5, no. 1, Part 3, pp. 2635–2640, 2018, https://doi.org/https://doi.org/10.1016/j.matpr.2018.01.043.

UNCORRECTED PROOF

20. A. P. Schaffarczyk, *Introduction to Wind Turbine Aerodynamics*. Cham, Switzerland: Springer International Publishing, 2024.
21. A. Angelovski and A. Dedinec, "Day-ahead forecasting for solar and wind electricity production using machine learning techniques," in *Proceedings of 20th International Conference on Informatics and Information Technologies - CIIT 2023*, May 2023, pp. 79–82.
22. M. Celeska Krstevska, K. Najdenkoski, V. Stoilkov, and V. Dimchev, "Modeling an optimal wind turbine layout by application of evolutional algorithms," in *Proceedings of 11th MAKO CIGRE Conference*, Oct. 2019, pp. 1–8, Accessed: Mar. 07, 2026. [Online]. Available: https://mako-cigre.mk/sovetuvanja/y/2019/en/index.html.
23. B. Hoxha, A. Kuriqi, and R. V. Filkoski, "Influence of seasonal air density fluctuations on wind speed distribution in complex terrains in the context of energy yield," *Energy Ecol. Environ.*, vol. 9, no. 2, pp. 175–187, Nov. 2024, https://doi.org/10.1007/s40974-023-00301-9.
24. S. Bogoevska, E. Chatzi, E. Dumova-Jovanoska, and R. Hoeffer, "Data-driven tool for structural health monitoring of operating wind turbines," *Scientific Journal of Civil Engineering*, vol. 8, no. 2, pp. 65–68, Dec. 2019, https://doi.org/10.55302/SJCE1982065b.
25. V. Mijakovski, M. Lutovska, and Z. Trajkovski, "Techno-economic analysis of the wind park Bogdanci in the Republic of Macedonia," *Thermal Science*, vol. 22, no. Suppl. 5, pp. 1449–1458, 2018, https://doi.org/10.2298/TSCI18S5449M.
26. K. Cheng, Z. Wang, Y. He, and G. Yang, "The Comparison of Theoretical Potential Application of Two Types of Wind Turbines in Northern Shaanxi," in *2012 Asia-Pacific Power and Energy Engineering Conference*, Mar. 2012, pp. 1–4, https://doi.org/10.1109/APPEEC.2012.6307134.
27. J. S. Chawla, S. Suryanarayanan, B. Puranik, J. Sheridan, and B. G. Falzon, "Efficiency improvement study for small wind turbines through flow control," *Sustainable Energy Technologies and Assessments*, vol. 7, pp. 195–208, Sep. 2014, https://doi.org/https://doi.org/10.1016/j.seta.2014.06.004.
28. A. Bensalah, G. Barakat, and Y. Amara, "Electrical Generators for Large Wind Turbine: Trends and Challenges," *Energies*, vol. 15, no. 18. MDPI, p. 6700, Sep. 2022, https://doi.org/10.3390/en15186700.
29. S. Rajamohan, A. Vinod, M. P. V. S. Aditya, H. G. Vadivudaiyanayaki, V. N. Nguyen, M. Arıcı, S. Nižetić, T. T. Le, R. Hidayat, and D. T. Nguyen, "Approaches in performance and structural analysis of wind turbines – A review," *Sustainable Energy Technologies and Assessments*, vol. 53, p. 102570, Oct. 2022, https://doi.org/https://doi.org/10.1016/j.seta.2022.102570.
30. K. A. Adeyeye, N. Ijumba, and J. Colton, "The Effect of the Number of Blades on the Efficiency of A Wind Turbine," *IOP Conf. Ser. Earth Environ. Sci.*, vol. 801, no. 1, p. 012020, Jun. 2021, https://doi.org/10.1088/1755-1315/801/1/012020.
31. V. H. Morcos, "Aerodynamic performance analysis of horizontal axis wind turbines," *Renew. Energy*, vol. 4, no. 5, pp. 505–518, Jul. 1994, https://doi.org/https://doi.org/10.1016/0960-1481(94)90213-5.
32. R. Zha, S. Wu, C. Cai, X. Liu, D. Wang, C. Peng, X. Feng, Q. Chen, X. Zhong, and Q. Li, "A Review on Performance Calculation and Design Methodologies for Horizontal-Axis Wind Turbine Blades," *Energies*, vol. 18, no. 2. MDPI, p. 435, Jan. 2025, https://doi.org/10.3390/en18020435.
33. S. Fayyad, A. Alawin, S. Abu-Ein, Z. Abulghanam, A. Alsabag, M. O. Al-Rawashdeh, M. Momani, and W. Momani, "Aerodynamics Analysis Comparison between NACA 4412 and NREL S823 Airfoils," *WSEAS TRANSACTIONS ON FLUID MECHANICS*, vol. 19, pp. 129–141, Apr. 2024, https://doi.org/10.37394/232013.2024.19.13.

UNCORRECTED PROOF

34. J. L. Tangier and D. M. Somers, "NREL Airfoil Families for HAWTs," Golden, Colorado, USA, Jan. 1995.
35. A. Björck, *Coordinates and calculations for the FFA-W1-xxx, FFA-W2-xxx, and FFA-W3-xxx series of airfoils for horizontal axis wind turbines*. Stockholm, Sweden: Aeronautical Research Institute of Sweden, 1990.
36. P. Fuglsang, I. Antoniou, K. S. Dahl, and H. Aa. Madsen, *Wind tunnel tests of the FFA-W3-241, FFA-W3-301 and NACA 63-430 airfoils*. Roskilde, Denmark: Riso National Laboratory, 1998.
37. W. A. Timmer and R. P. J. O. M. van Rooij, "Summary of the Delft University Wind Turbine Dedicated Airfoils," *J. Sol. Energy Eng.*, vol. 125, no. 4, pp. 488–496, Nov. 2003, https://doi.org/10.1115/1.1626129.
38. P. Fuglsang, I. Antoniou, C. Bak, and H. Madsen, *Wind Tunnel Test of the RIS0-1 Airfoil*. Roskilde, Denmark: Riso National Laboratory, 1998.
39. P. Fuglsang, K. Dahl, and I. Antoniou, *Wind tunnel tests of the Risø-A1-18, Risø-A1-21 and Risø-A1-24 airfoils*. Roskilde, Denmark: Riso National Laboratory, 1999.
40. J. Xu, Z. Han, X. Yan, and W. Song, "Aerodynamic Design of Megawatt Wind Turbine Blades with NPU-WA Airfoils," *IOP Conf. Ser. Earth Environ. Sci.*, vol. 495, no. 1, p. 012018, Apr. 2020, https://doi.org/10.1088/1755-1315/495/1/012018.
41. M. Selig, J. Guglielmo, A. Broeren, and P. Giguere, *Summary of Low Speed Airfoil Data*, vol. 1. Virginia Beach, Virginia, USA: SoarTech Publications, 1995.
42. Y. Celik, "A Comparative Aerodynamic Analysis of NACA and NREL Aerofoils for Darrieus Turbines Using CFD," *International Journal of Innovative Engineering Applications*, vol. 6, no. 1, pp. 111–117, Jun. 2022, https://doi.org/10.46460/ijiea.1075684.
43. M. Hady, "A Comparative Study for Different Shapes of Airfoils," *Journal of Advanced Research in Fluid Mechanics and Thermal Sciences*, vol. 69, no. 1, pp. 34–45, Apr. 2020, https://doi.org/10.37934/arfmts.69.1.3445.
44. A. Ghosh, "Comparative Analysis of NACA Airfoil Series Performance using Computational Fluid Dynamics (CFD)," *Journal of Emerging Technologies and Innovative Research (JETIR)*, vol. 11, no. 5, pp. 689–708, May 2024, Accessed: Mar. 08, 2026. [Online]. Available: https://www.jetir.org/papers/JETIR2405079.pdf.
45. A. Singh and R. Sharma, "Review paper on CFD analysis of different NACA airfoil series," *Journal of Emerging Technologies and Innovative Research (JETIR)*, vol. 11, no. 3, Mar. 2024, Accessed: Mar. 08, 2026. [Online]. Available: https://www.jetir.org/papers/JETIR2403948.pdf.
46. T. Batu and H. Lemu, "Comparative Study of the Effect of Chord Length Computation Methods in Design of Wind Turbine Blade," in *Advanced Manufacturing and Automation IX (IWAMA 2019). Lecture Notes in Electrical Engineering*, vol. 634, Singapore: Springer, 2020, pp. 106–115.
47. C.-J. Bai and W.-C. Wang, "Review of computational and experimental approaches to analysis of aerodynamic performance in horizontal-axis wind turbines (HAWTs)," *Renewable and Sustainable Energy Reviews*, vol. 63, pp. 506–519, Sep. 2016, https://doi.org/https://doi.org/10.1016/j.rser.2016.05.078.
48. Z. Sun, J. Chen, W. Z. Shen, and W. J. Zhu, "Improved blade element momentum theory for wind turbine aerodynamic computations," *Renew. Energy*, vol. 96, pp. 824–831, Oct. 2016, https://doi.org/https://doi.org/10.1016/j.renene.2016.05.035.
49. A. Bouhelal, A. Smaïli, O. Guerri, and C. Masson, "Comparison of BEM and Full Navier-Stokes CFD Methods for Prediction of Aerodynamics Performance of HAWT Rotors," in *2017 International Renewable and Sustainable Energy Conference (IRSEC)*, Dec. 2017, pp. 1–6, https://doi.org/10.1109/IRSEC.2017.8477247.

UNCORRECTED PROOF

50. G. Bangga, "Comparison of blade element method and CFD simulations of a 10 MW wind turbine," *Fluids*, vol. 3, no. 4, p. 73, Oct. 2018, https://doi.org/https://doi.org/10.3390/fluids3040073.
51. S. Yang, M. Zhang, Y. Feng, H. Jia, N. Zhao, and Q. Chen, "Research on the Improvement of BEM Method for Ultra-Large Wind Turbine Blades Based on CFD and Artificial Intelligence Technologies," *Fluids*, vol. 10, no. 5, p. 112, Apr. 2025, https://doi.org/10.3390/fluids10050112.
52. D. Marten, "QBlade: A Modern Tool for the Aeroelastic Simulation of Wind Turbines vorgelegt von," PhD, TU Berlin, Berlin, Germany, 2020.
53. A. Kumar, A. Tahasildar, A. Naidu, M. Suhail, and P. Divakar, "Design and Analysis of Horizontal Axis Small Wind Turbine for Low Wind Velocity Using QBlade," *Journal of Mines, Metals and Fuels*, vol. 71, no. 12, pp. 2554–2560, Dec. 2023, https://doi.org/10.18311/jmmf/2023/36540.
54. T. Batu, H. Lemu, and B. Sirhabizuh, "Study of the Performance of Natural Fiber Reinforced Composites for Wind Turbine Blade Applications," *Advances in Science and Technology Research Journal*, vol. 14, no. 2, pp. 67–75, Jun. 2020, https://doi.org/10.12913/22998624/118201.
55. D. E. Husaru, P. D. Bârsănescu, and D. Zahariea, "Effect of yaw angle on the global performances of Horizontal Axis Wind Turbine - QBlade simulation," *IOP Conf. Ser. Mater. Sci. Eng.*, vol. 595, no. 1, p. 012047, Sep. 2019, https://doi.org/10.1088/1757-899X/595/1/012047.
56. M. Alaskari, O. Abdullah, and M. H. Majeed, "Analysis of Wind Turbine Using QBlade Software," *IOP Conf. Ser. Mater. Sci. Eng.*, vol. 518, no. 3, p. 32020, May 2019, https://doi.org/10.1088/1757-899X/518/3/032020.
57. W. K. Abbas, M. Abbasalizadeh, and S. Khalilarya, "Optimizing of horizontal axis wind turbine blades using MATLAB-based blade element momentum theory with validation in QBlade and CFD software," *Wind Engineering*, vol. 49, no. 4, pp. 968–993, Aug. 2024, https://doi.org/10.1177/0309524X241293140.
58. M. R. Islam, L. Bin Bashar, and N. S. Rafi, "Design and Simulation of A Small Wind Turbine Blade with Qblade and Validation with MATLAB," in *2019 4th International Conference on Electrical Information and Communication Technology (EICT)*, Dec. 2019, pp. 1–6, https://doi.org/10.1109/EICT48899.2019.9068762.
59. N. Noronha and K. Munishamaiah, "Design and analysis of micro horizontal axis wind turbine using MATLAB and QBlade," *International Journal of Advanced Science and Technology*, vol. 29, no. 10S, pp. 8877–8885, 2020.
60. J. G. Leishman, "Aerodynamics of Horizontal Axis Wind Turbines," in *Advances in Wind Energy Conversion Technology*, M. Sathyajith and G. S. Philip, Eds. Berlin Heidelberg: Springer, 2011, pp. 1–69.
61. T. Burton, N. Jenkins, E. Bossanyi, D. Sharpe, and M. Graham, *Wind Energy Handbook*, 3rd ed. Chichester, UK: John Wiley & Sons, 2021.
62. DNV/Risø, *Guidelines for Design of Wind Turbines*, 2nd Edition. Roskilde, Denmark: Risø National Laboratory, 2002.
63. P. Jamieson, *Innovation in Wind Turbine Design*, 2nd Edition. Chichester, UK: John Wiley & Sons, 2018.
64. M. Debbache, M. Hazmoune, S. Derfouf, D.-A. Ciupageanu, and G. Lazaroiu, "Wind Blade Twist Correction for Enhanced Annual Energy Production of Wind Turbines," *Sustainability*, vol. 13, no. 12, p. 6931, Jun. 2021, https://doi.org/10.3390/su13126931.
65. G. Ingram, *Wind Turbine Blade Analysis Using the Blade Element Momentum Method*. Durham, UK: Durham University, 2011.
66. S. Duran, "Computer-Aided Design of Horizontal-Axis Wind Turbine Blades," MSc, Middle East Technical University, 2005.

UNCORRECTED PROOF

67. VESTAS, "2 MW Platform." https://docs.wind-watch.org/2_MW_Product_Brochure_Vestas-2MW.pdf (accessed Mar. 07, 2026).
68. C. Bak, F. Zahle, R. D. Bitsche, T. Kim, A. Yde, L. C. Henriksen, M. H. Hansen, J. P. A. A. Blasques, M. Gaunaa, and A. Natarajan, "Description of the DTU 10-MW Reference Wind Turbine," in *Technical Report DTU Wind Energy Report-I-0092*, Roskilde, Denmark: Danish Technical University, DTU Wind Energy Roskilde, 2013.
69. E. Gaertner, J. Rinker, L. Sethuraman, F. Zahle, B. Anderson, G. E. Barter, N. J. Abbas, F. Meng, P. Bortolotti, W. Skrzypinski, G. N. Scott, R. Feil, H. Bredmose, K. Dykes, M. Shields, C. Allen, and A. Viselli, *IEA Wind TCP Task 37: Definition of the IEA 15-Megawatt Offshore Reference Wind Turbine*. Golden, CO, USA: National Renewable Energy Laboratory (NREL), 2020.
70. J. Jonkman, S. Butterfield, W. Musial, and G. Scott, *Definition of a 5-MW Reference Wind Turbine for Offshore System Development*. Golden, CO, USA: National Renewable Energy Laboratory (NREL), 2009.
71. M. Vitulano, D. De Tavernier, G. De Stefano, and D. von Terzi, "Numerical Analysis of Transonic Flow over the FFA-W3-211 Wind Turbine Tip Airfoil," *Wind Energy Science*, vol. 10, no. 1, Jan. 2025, https://doi.org/10.5194/wes-2024-47.
72. S. Chellini, D. De Tavernier, and D. von Terzi, "Experimental characterization of dynamic stall of the FFA-W3-211 wind turbine airfoil," *Wind Energy Science*, vol. 11, no. 3, pp. 753–769, Mar. 2026, https://doi.org/10.5194/wes-11-753-2026.
73. L. Viterna and D. Janetzke, *Theoretical and experimental power from large horizontal-axis wind turbines*. Cleveland, Ohio, USA: National Aeronautics and Space Administration (NASA), 1982.
74. M. Grujicic, G. Arakere, E. Subramanian, V. Sellappan, A. Vallejo, and M. Ozen, "Structural-Response Analysis, Fatigue-Life Prediction, and Material Selection for 1 MW Horizontal-Axis Wind-Turbine Blades," *J. Mater. Eng. Perform.*, vol. 19, no. 6, pp. 790–801, Aug. 2010, https://doi.org/10.1007/s11665-009-9558-8.
75. P. Y. Andoh, A. Agyei-Agyemang, P. O. Tawiah, C. K. K. Sekyere, and C. M. Asante, "Development of Composite Material for Wind Turbine Blades," *Journal of Applied Engineering and Technological Science (JAETS)*, vol. 2, no. 2, pp. 139–150, Jul. 2021, https://doi.org/10.37385/jaets.v2i2.211.
76. X. Cheng, B. Du, J. He, W. Long, G. Su, J. Liu, Z. Fan, and L. Chen, "A review of thermoplastic composites on wind turbine blades," *Compos. B Eng.*, vol. 299, p. 112411, Jun. 2025, https://doi.org/10.1016/j.compositesb.2025.112411.

UNCORRECTED PROOF